An evaluation method for SAXS-patterns of fibrillar two-phase systems containing oriented particles of moderate anisotropy and short range correlation

N. Stribeck

Institut für Technische und Makromolekulare Chemie, Universität Hamburg, Hamburg, F.R.G.

Abstract: Starting from the theoretical background of Rulands interface distributions, an evaluation method for small angle x-ray patterns arising from oriented fibrillar two-phase structures is proposed. If the fibril contains highly oriented particles with only moderate anisotropy and if the correlations between those particles within the fibril are of short range only, every axial section of the scattering pattern shows a one dimensional Porod law. A procedure of successive model confinement using the well known tools of nonlinear regression analysis is described. The result of such an analysis for the scattering pattern of an oil diluted SBS block copolymer recorded with synchrotron radiation under first-cycle stretching is reported. At $\lambda = 4$ . . four contributions to the scattering pattern could be identified: a) fibrils containing well-defined cylinders standing upright; b) fibrils containing lying cylinders under destruction; c) stretched-out polybutadiene chains, connecting two polystyrene cylinders and causing the observable layer line pattern; and d) stretched-out polybutadiene chains looping through the neighboring PS domain and returning to their starting domain. In addition, a simple method for determining the height-to-diameter ratio of cylinders from the form factor envelope is proposed.

Key words: SAXS, oriented fibrils, block copolymers, drawing, synchrotron radiation.

1. Introduction

Under first-cycle stretching of oil-diluted SBS block copolymers Polizzi and Bösecke [1] observed SAXS layer line patterns within an ellipsoidal particle form factor. Figure 1 shows one of the most detailed patterns, collected with a Vidicon-System at the Hamburg synchrotron radiation laboratory (HASYLAB). Due to the large blind spot of the primary beam stop, it is not possible to observe the layer lines on the rotational axis of the pattern. SAXS studies of similar samples under strain recently have been published by Pakula et al. [2] and Séguéla and Prud'homme [3].

The layer lines suggest that a perfectly oriented one-dimensional structure does exist. A simple model to explain the ellipsoidal envelope is that of highly oriented cylindrical particles with a height-to-diameter ratio of about 2. Due to the dominant form factor Porod's law cannot be found in the scattering pattern. Therefore a new theoretical approach shall be put forward, adapted to a regression analysis in reciprocal space.

2. Theoretical

2.1 General definitions

Let $\vec{r}$ be the vector in physical space and $\vec{s}$ the scattering vector in reciprocal space with $|\vec{s}| = 2\frac{\sin\theta}{\lambda} \cdot \lambda$ is the wavelength of radiation, 2θ the scattering angle. Let $\Delta\varrho(\vec{r})$, the electron density difference, be defined by $\Delta\varrho(\vec{r}) = \varrho(\vec{r}) - \langle\varrho(\vec{r})\rangle_V$. $\langle\ \rangle_V$ denotes the average over the irradiated volume. Then the scattering intensity $I(\vec{s})$, arising from $\Delta\varrho(\vec{r})$, is given by

$$I(\vec{s}) = |\mathcal{F}[\Delta\varrho(\vec{r})]|^2 \qquad (1)$$

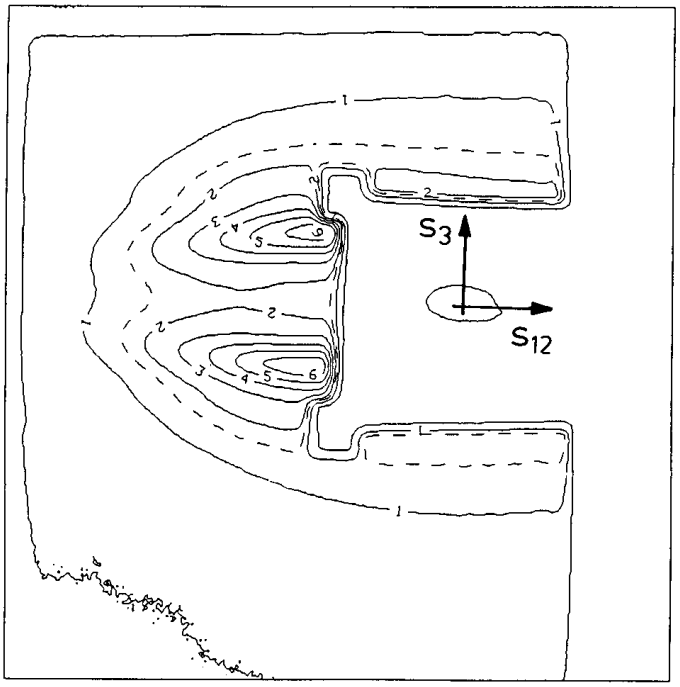

Fig. 1. SAXS-contour plot of an oil diluted (50 wt% paraffinic mineral oil) SBS block copolymer sample under first-cycle stretching at a draw ratio of $\lambda = 4$. Measurement with synchrotron radiation at Hasylab, Hamburg

with the Fourier transform $\mathcal{F}$ [ ] being defined as

$$\mathcal{F}\,[g\,(\vec{r})]\,(\vec{s}) = \iiint g\,(\vec{r}) \cdot e^{2\pi i \vec{r}\vec{s}}\, d^3 r\,. \qquad (2)$$

In this work $I(\vec{s})$ is assumed to show cylindrical symmetry

$$I(\vec{s}) = I(s_{12}, s_3) \qquad (3)$$

with s_{12} defining the radial and s_3 the axial component of the scattering vector. Under this assumption a convenient scattering curve I_{sc} is a section parallel to one of the cylindrical coordinates

$$I_{sc}(s_3) = I(s_{12}, s_3)\,|_{s_{12}\,=\,\text{const.}}$$

or

$$I_{sc}(s_{12}) = I(s_{12}, s_3)\,|_{s_3\,=\,\text{const.}}\,. \qquad (4)$$

The sections through the origin of reciprocal space ("origin sections") shall be written as

$$[I(\vec{s})]_{s_{12}} := I(s_{12}, s_3)\,|_{s_{12}\,=\,0} = I(0, s_3)$$

$$[I(\vec{s})]_{s_3} := I(s_{12}, s_3)\,|_{s_3\,=\,0} = I(s_{12}, 0)\,. \qquad (5)$$

Furthermore, if $I(s_{12}, s_3) = g\,(s_{12}) \cdot h\,(s_3)$, is product separable, any of the sections according to Eq. (4) is proportional to the corresponding origin section according to Eq. (5).

2.2 *The scattering of a single cylinder*

Cylinders represent an appropriate model to describe particles with moderate anisotropy, the decrease of the height-to-diameter ratio describing the change from rods to disks (finite lamellae).

In real space let us assume a single cylinder of height h_c and diameter d_c, oriented in r_3-direction. The electron density of the cylinder is assumed to be 1 and that of the surrounding matrix to be 0. From Eq. (1) it follows for the cylinders scacttering intensity $I_c(\vec{s})$

$$I_c(\vec{s}) = V_c^2 \cdot \text{Jinc}^2\,(\pi\, d_c\, s_{12}) \cdot \text{sinc}^2\,(\pi\, h_c\, s_3) \qquad (6)$$

with V_c being the cylinder volume, sinc $(x) :=$ sin $(x)/x$ and Jinc $(x) := 2\,J_1\,(x)/x$, where $J_1\,(x)$ is the Bessel function of first kind and first order.

If one identifies the main contribution to the ellipsoidal form factor with a function of the type $I_c(\vec{s})$, the experiment mentioned in the introduction shows that its axial term Jinc^2 $(\pi\, d_c\, s_{12})$ as well as its radial term sinc^2 $(\pi\, h_c\, s_3)$ are only observable in the interval $(0, s_z)$. s_z denotes the first zero of each term. For larger s the scattering pattern is governed by statistical noise, the weak tail of the terms discussed and density fluctuations within the phases.

Comparing the shapes of Jinc^2 $(\pi\, d_c\, s)$ and sinc^2 $(\pi\, h_c\, s)$ (see Fig. 2), it turns out that it is impossible to dis-

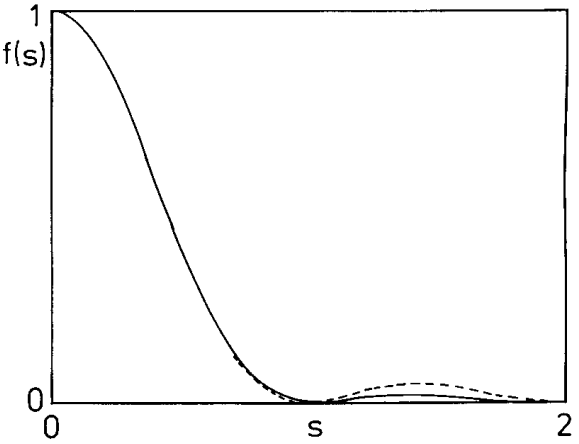

Fig. 2. Formfactor $f(\vec{s}) =$ Jinc^2 $(1.17\,\pi\, s_{12}) \cdot$ sinc^2 $(\pi\, s_3)$ of a cylinder with diameter $d_c = 1.17$ and heigth $h_c = 1$ in radial (– – –) and in axial (——) "origin sections". In the radial section s is defined $s := s_{12}$, and $s := s_3$ for the axial section

criminate between both functions in the observable interval $[0, s_z]$

$$\text{Jinc}^2(\pi\, d_c\, s) \approx \text{sinc}(\pi\, h_c\, s) \text{ for } d_c = 1.17 \cdot h_c \quad (7)$$

with an accuracy of better than 0.5 % of the maximal value.

To get the dimensions of the cylinder, one thus would have to find the first zeros of the form factor in both s_{12} and s_3 directions, s_{12z} and s_{3z}. Height and diameter of the cylinder then are given by

$$h_c = 1/s_{3z}$$
$$d_c = 1.22/s_{12z}. \quad (8)$$

In practice it will be difficult to determine h_c and d_c by searching s_{12z} and s_{3z}. This is due to decreasing signal-to-noise ratio in the outer part of the scattering pattern and modulation by interparticular scattering in the inner part. Anyway, the affinity of shape according to Eq. (7) at least allows the ratio h_c/d_c to be determined from any outer ellipsoidal contour line. Let a_{12} be the length of its half axis in s_{12}-direction, and a_3 the length of its half axis in s_3-direction, it follows that

$$\frac{h_c}{d_c} = \frac{a_{12}}{1.17 \cdot a_3}. \quad (9)$$

Of course, for an ensemble of cylinders this is only correct if the cylinders are highly oriented with little variation of their dimensions.

2.3 *The scattering of fibrils*

If the SAXS pattern shows cylindrical symmetry, the observed reflections being continuous layer lines, the interparticular scattering in the simplest case can be described in terms of a one-dimensional model of particles arranged within a fibril, neglecting any correlations among different fibrils. The information on the fibrillar morphology is then contained in the section through the scattering pattern perpendicular to the layer lines, $I_{fc}(s_3)$

$$I_{fc}(s_3) := [I(\vec{s})]_{s_{12}}. \quad (10)$$

Under the assumption of perfect orientation one can directly identify

$$I_{fc}(s_3) = I_1(s_3), \quad (11)$$

the one-dimensional scattering curve caused by cylinders arranged in a fibril. Ruland's theory of interface distribution functions [4] is able to describe $I_1(s_3)$ without any assumptions on the length of the fibril or the statistics of cylinders and gaps in between. In an earlier work [5] it was shown that the distance distributions $h_i(r_3)$ from that theoretical approach could be approximated by Gaussian functions

$$h_i(r_3) = \frac{1}{\sigma_i \sqrt{2\pi}} \exp\left(-\frac{(r_3 - d_i)^2}{2\sigma_i^2}\right) \quad (12)$$

with σ_i, the variance of the Gaussian distribution, describing the width of the distance distribution and d_i the mean distance between an arbitrary phase boundary and its i-th neighbor.

This approximation led to a compact formula in reciprocal space, describing $I_1(s_3)$ by a sum of attenuated cosine terms, multiplied with Porod's law

$$I_1(s_3) = A_p/s_3^2 \cdot [1 - \sum_i w_i\, H_i(s_3)]$$
$$H_i(s_3) = \cos(2\pi\, d_i\, s_3) \cdot \exp(-2\pi^2\, \sigma_i^2\, s_3^2) \quad (13)$$

with A_p being the asymptote of the one-dimensional Porod law and $H_i(s_3) = \mathcal{F}[h_i(r_3)]$. The parameters w_i (taking into account the multiplicity and sign of the h_i) and d_i describe the general model of the one-dimensional structure. If one decides on number and succession of basic distinguishable heights in the one-dimensional structure, all the w_i are given and the d_i can be reduced to those basic heights (e.g., the mean height of the cylinders and the mean height of the gaps in the fibril). As one can see, $I_1(s_3)$ is successively approximated by the terms in the sum.

In this general model the increase of the σ_i describes the loss of correlation with increasing distance from any arbitrary phase boundary. A further reduction of the parameter set can be accomplished by assuming a statistical model for the cylinders in the fibril.

2.4 *Infinite fibrils*

To describe an infinite fibril, one has to extend the sum in Eq. (13) to infinity. As mentioned above, the

first step in reducing the parameter set is to decide on the number and succession of basic heights.

2.4.1 Statistical models for two basic heights in the fibril

Let us first discuss the most simple case of two basic heights in the fibril and name those the mean cylinder height, h_c, and the mean gap height, h_g. Then for the parameters w_i and d_i it follows [5]

$$\begin{aligned} w_i &= 1 && \text{for } i \neq 3n, \\ w_i &= -2 && \text{for } i = 3n. \\ d_i &= n(h_c + h_g) && \text{for } i = 3n, \\ d_i &= n(h_c + h_g) + h_c && \text{for } i = 3n + 1, \\ d_i &= n(h_c + h_g) + h_g && \text{for } i = 3n + 2. \end{aligned} \quad (14)$$

Thus all the d_i are expressed in terms of h_c and h_g.

A model for fibrillar statistics with good long range order is that of an "inhomogeneous system with exact lattice" (Kratky, cited in Porod [6]), where each fibril is assumed to be a perfect lattice with the lattice constant varying from fibril to fibril. In a previous paper, Ruland [5] named this model a "homogeneous L distribution" and gave the formulas reducing the σ_i for this and the models to be described in the following.

The model of a one-dimensional paracrystalline lattice assumes the lattice constant and the height h_c to vary independently within each fibril. The poorest model inherent long range order is represented by the stacking statistics, where h_c and h_g vary independently. For the last two models equations avoiding an infinite sum can be given [7]

$$I_1(s) = A_p/s^2 \cdot [1 - G_b(s) + G_a(s) \cdot G_L(s)] \quad (15)$$

with $G_b(s)$ denoting a background, $G_a(s)$ an attenuating factor, and $G_L(s)$ a lattice factor. For the ease of notation we define

$$A_i(s) := \exp(-2\pi^2 \sigma_i^2 s^2) \text{ and}$$

$$O_i(s) := \cos(2\pi d_i s) \quad (16)$$

as simple attenuating and oscillating terms. Then for the paracristalline lattice statistics the G-functions of Eq. (15) are given by

$$G_b(s) = H_1(s) = O_1(s) \cdot A_1(s)$$

$$G_a(s) = [1 - O_1(s)] \cdot A_1^{1/2}(s)$$

$$G_L(s) = \frac{1 - A_3^2(s)}{1 + A_3^2(s) - 2 \cdot H_3(s)} - 1 \quad (17)$$

and for stacking statistics

$$G_b(s) = 1 + H_1(s) + H_2(s)$$

$$G_a(s) = 1 - \frac{A_3(s)}{1 - A_3^2(s)} \cdot [A_1(s) \cdot O_4(s) + A_2(s) \cdot O_5(s) - A_3(s) \cdot [H_1(s) + H_2(s)]]$$

$$G_L(s) = \frac{1 - A_3^2(s)}{1 + A_3^2(s) - 2 \cdot H_3(s)} \cdot \quad (18)$$

Since the summation does not need to be performed, Eq. (15) can be computed faster than Eq. (13). On the other hand, Eq. (13) together with the conditions according to Eq. (15) can be used to choose the appropriate statistical model for a given set of data. For that purpose regression analysis with free parameters σ_i can serve as a tool.

If the general model is not adaptable to the data, the series of σ_i will be of no physical sense (e.g., if σ_3 were very high and σ_6 low, it would be rather improbable to find the next cylinder close to the mean distance from the first one, while the cylinder after the next were to be found within a narrow range of distance). In this case there will be more than two basic heights either within each fibril or within a multi-component fibrillar system.

2.4.2 General model for one cylinder height and a bimodal gap

A very simple model for a fibril with more than two basic heights is made by the assumption of two different gaps in the fibril (see Fig. 3a). The short and long indices of the first 16 distinguishable distances as well as the weights w_i are given in Table 1. Because of the fact that the repetition unit in the fibril contains two particles of each kind, the absolute value of the w_i is only half the number of realization possibilities in the fibril. The sums reducing the d_i to the three basic

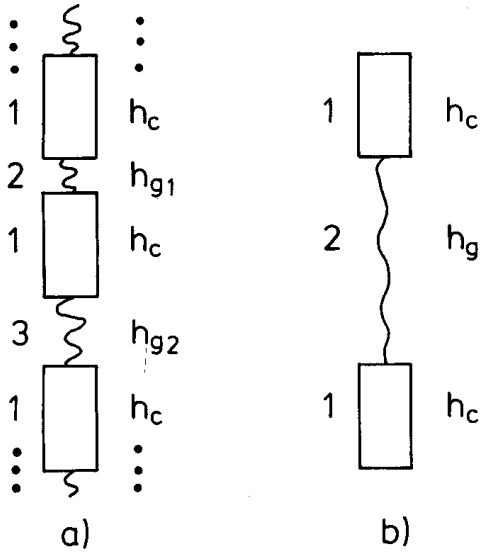

Fig. 3. a) Model of an infinite stack with three basic lengths: h_c (cylinder height), h_{g1} and h_{g2} (gap heights); b) model of a finite fibril containing just two cylinders. If the gap height is very precise over the ensemble, the fibril is called a string

Table 1. The first 16 distances of a one-dimensional model with three basic distances. The long index describes the series of the basic distances; w_i is the weight according to Eq. (13)

i	long index	w_i
1	(1)	1.0
2	(2)	0.5
3	(3)	0.5
4	(12)	−1.0
5	(13)	−1.0
6	(121)	0.5
7	(131)	0.5
8	(213)	1.0
9	(1213)	−2.0
10	(12131)	1.0
11	(21312)	0.5
12	(31213)	0.5
13	(121312)	−1.0
14	(131213)	−1.0
15	(1213121)	0.5
16	(1312131)	0.5

heights can easily be deduced from the long index of the distance, where 1 means a height of h_c, 2 a height of h_{g1}, and 3 a height of h_{g2}.

2.5 Finite fibrils

Equation (13) describes finite fibrils, if the sum is limited. For the most simple case we only take the first term of the sum and get the scattering of an ensemble of isolated particle heights. The variation of those heights is described by the parameter σ_1. Considering just one single cylinder of height h_c (and trivially $\sigma_1 = 0$), Eq. (13) exactly represents the radial section of Eq. (6)

$$[I_c(\vec{s})]_{s_{12}} = V_c^2 \cdot \mathrm{sinc}^2\,(\pi\, h_c\, s_3) \equiv A_p/s_3^2 \cdot [1 - \cos\,(2\pi\, h_c\, s_3)] \qquad (19)$$

with $A_p = V_c^2/(2\pi^2\, h_c^2)$.

Now the scattering of two cylinders of height h_c with a gap h_g in between (see Fig. 3b) shall be computed. Following the geometrical scheme to determine weights of all the distances to be found in the model, Eq. (13) becomes

$$I_1(s_3) = A_p/s_3^2 \cdot [1 - \cos[2\pi\, s_3\, h_c] \cdot \exp[-2\pi^2\, \sigma_1^2\, s_3^2] - \frac{1}{2} \cdot \cos\,[2\pi\, s_3\, h_g] \cdot \exp\,[-2\pi^2\, \sigma_2^2\, s_3^2] + \cos\,[2\pi\, s_3(h_c + h_g)] \cdot \exp\,[-2\pi^2\, \sigma_3^2\, s_3^2] - \frac{1}{2} \cdot \cos\,[2\pi\, s_3\,(h_c + h_g + h_c)] \cdot \exp\,[-2\pi^2\, \sigma_4^2\, s_3^2]]\,. \qquad (20)$$

Let a "string" be defined by the assumption that the height of the spacer gap is well defined ($\sigma_2 \approx 0$), while both the h_c in the ensemble vary independently. For an example, let h_g be nine times h_c, and σ_1 (i.e., the variation of the h_c) be very high ($\sigma_1/h_c = 0.5$). Then Fig. 4 shows the comparison of the curves $s_r^2 \cdot I_1(s_r)$ ($s_r = s_3 \cdot (h_c + h_g)$) between the string and an infinite stack with the same parameters. As one can see, the scattering of the string shows reflections less sharp with their amplitude modulated in a significantly different way than those of the infinite stack.

2.6 Imperfect orientation of particles with moderate anisotropy

As soon as the orientation of the assumed fibrils is no longer perfect, for large s_3 we will not find the one-

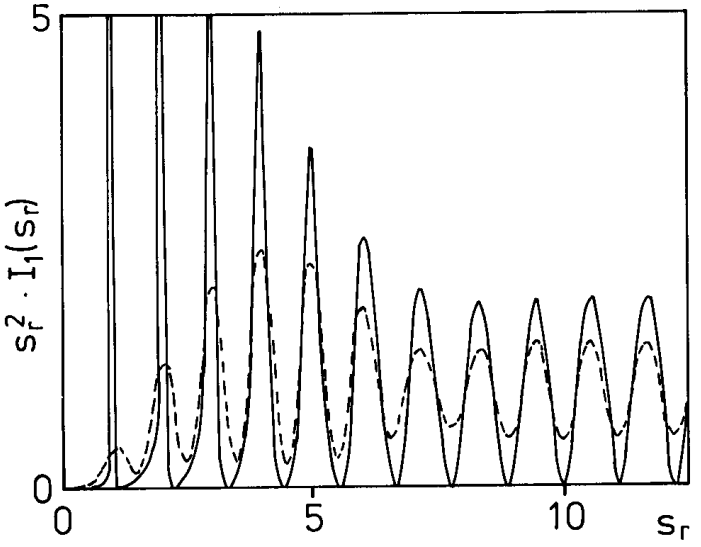

Fig. 4. Interference functions $s_r^2 \cdot I_1(s_r)$ for fibrils with perfect gap length. (——): infinite stacking model; (- - -): finite string model. $s_r = s_3 \cdot (h_c + h_g)$, reduced length of scattering vector

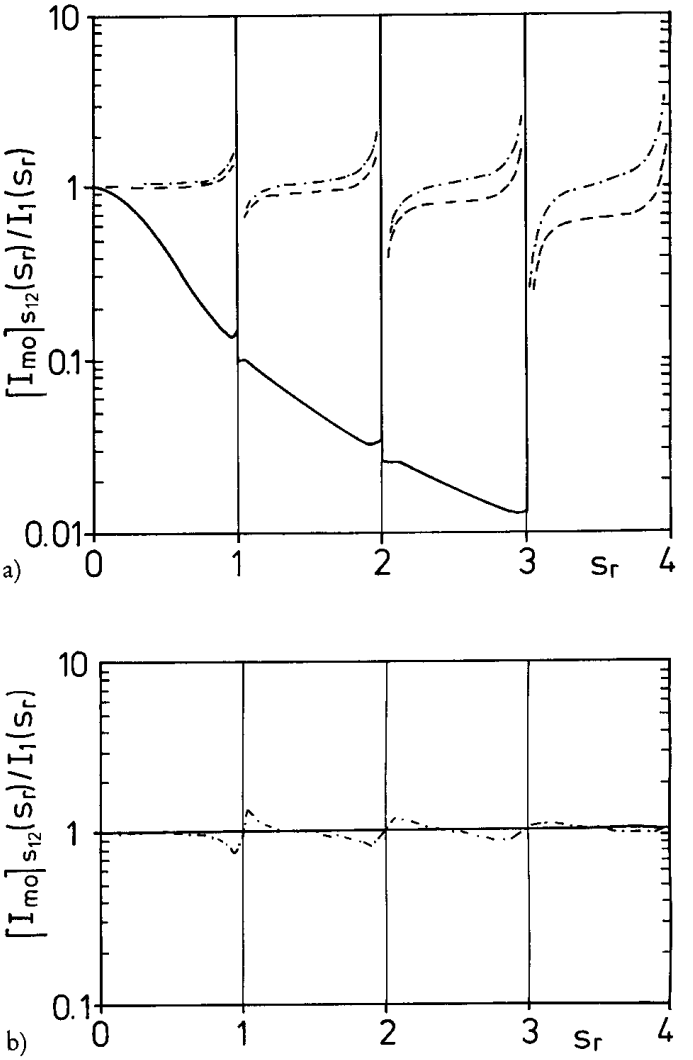

Fig. 5. a) Effect of misorientation on the axial component of the structural factor of cylinders with various height-to-diameter ratios h_c/d_c. (-·-·-): rod, ($h_c/d_c = 10$). (- - -): $h_c/d_c = 1$. (——): lamella, ($h_c/d_c = 0.1$). $s_r = s_3 \cdot h_c$. b) Effect of misorientation on the axial component of fibrillar scattering. $h_c/d_c = 2$, $h_g = 4 \cdot h_c$, $\sigma_1 = 0$ (all cylinders identical). (-·-·-): $\sigma_2 = h_g/10$ (long-range correlation). (——): $\sigma_2 = h_g/2$ (short-range correlation). $s_r = s_3 \cdot (h_c + h_g)$. Curves obtained by numerical integration. Integral width of pole figure: $2\alpha = 20°$

dimensional Porod law with a decrease proportional to s_3^{-2}, as intended by Eq. (13), but find the known decrease of the three-dimensional Porod law proportional to s_3^{-4}. For small s_3, on the other hand, a significant change of the scattering curve due to the solid angle average will not occur (Porod [8]). The amount of the effect for small values of s_3 strongly depends on the amount of misorientation and on the anisotropy of the base particles. The form factor of spheres obviously will not be altered, while infinite lamellae can be considered to follow the s_3^{-4} law in the whole observable interval.

Let us consider cylindrical particles with their principal axes homogeneously smeared out over a cone opening of $2\alpha = 20°$. Then the normalized axial section through the intensity pattern under misorientation, $[I_{mo}]_{s_{12}}$, is caused by averaging the linear scattering intensity I_1. For the following considerations the normalization shall be given by

$$[I_{mo}]_{s_{12}}(s_3 = 0) = I_1(s_3 = 0). \tag{21}$$

Now the effect of misorientation on the axial section of the scattering curve can be described by the ratio $[I_{mo}]_{s_{12}}/I_1$. Figure 5a shows this ratio for the pure structural factor of cylindrical particles with various h_c/d_c-ratio, plotted vs a reduced scattering vector $s_r = h_c \cdot s_3$. The curves were obtained by numerical integration. They show that the particle least anisotropic ($h_c/d_c = 1$) is very similar to a rod ($h_c/d_c = 10$). Misorientation for both particles causes the peaks to shift and become asymmetric rather than causing the curve as a whole to follow an additional s_r^{-2} law. On the other hand, for lamellae ($h_c/d_c = 0.1$), misorientation causes $[I_{mo}]_{s_{12}}/I_1$ to behave like a Lorentz function even in the considered interval of the scattering curve.

Now let us assume an ensemble of identical cylinders with $h_c/d_c = 2$, close to the value suggested by experiment. Let those cylinders be arranged in fibrils, perfectly oriented with respect to the fibrillar axes, and let misorientation be caused by fluctuations of the fibrillar axes as a whole. Let the gaps follow stacking statistics, the mean height of the gaps being $h_g = 4 \cdot h_c$. Then Fig. 5b shows the effect of misorientation ($2\alpha = 20°$) for various amounts of long range order in the fibril. Even for rather a good long range order ($\sigma_g = 0.1 \cdot h_g$) the effect of misorientation seems negligible. Thus we can approximate

$$[I_{mo}]_{s_{12}}(s_3) = c \cdot I_1(s_3) \tag{22}$$

with c being a constant.

2.7 *Non-origin sections*

In the case of a general section perpendicular to the layer lines, not containing the origin of reciprocal space, it is not easy to carry out the solid angle integration to compute the effect of misorientation. But if misorientation is small enough and the section is chosen as close as possible to the origin of reciprocal space, it should be allowed to transfer the result for the origin section (Eq. (22)) to the non-origin section as well.

In the latter case the constant of proportionality, c, will additionally be reduced by the radial term of the fibrillar scattering. Thus, considering a multi-component fibrillar system, it will be impossible to gain information on the true fraction of each component without additional assumptions on degree of orientation and fibrillar diameter for each component.

3. Regression analysis tools

Regression analysis was carried out using the Simplex algorithm of Caceci and Cacheris [9]. To estimate the quality of the fit, the program was extended by several procedures according to Draper and Smith [10]

– Computation of the asymptotic correlation matrix, yielding information on parameter correlation (to avoid overparametrization);

– Computation of the asymptotic intervals of confidence for each parameter value;

– Plot of the estimation error (to avoid underparametrization);

– Plots of data and fitted curve.

For every tested model each data set was processed at least twice to avoid a random termination of the algorithm. To avoid regression to a relative minimum, the residual sum of squares for a series of curves was demanded to be of the same order of magnitude. If not fulfilled, starting values were varied (a "series of curves" means same sample, varying elongation). If parameters were varied towards zero, they were removed from the model. Afterwards a computation with the simpler model was carried out.

4. Example of data analysis

The scattering pattern shown in Fig. 1 now shall be used to explain the special process of regression analysis. The sample is a SBS block copolymer spun cast from toluene solution at the Chemical Research Institute (ICECHIM), Bucharest, Romania [11]. The sample contains 50 wt% of a highly paraffinic mineral oil fraction. The molecular weights M_n[g/mole] of the blocks are 21 200–80 800–21 200.

The data set is made up from a section in s_3-direction near the edge of the primary beam stop. One-half of the 256 channels is disturbed because of cutting the edge of the beamstop, and a few channels in the outer part show a nonlinearity, possibly due to wear of the Vidicon target. For that reasons the final set covers 92 points of data in the interval $s_3 \in (0, 0.024 \cdot \text{nm}^{-1}]$. Data preprocessing only involves background correction and normalization to sample thickness, primary beam intensity and absorption, as described in [1]. Wavelength of synchrotron radiation was $\lambda_w = 0.15$ nm. Data points were not smoothed, so that the intervals of confidence, calculated for every parameter by the regression algorithm, take into account the statistical noise due to counting statistics.

According to Eq. (13) it seems appropriate to multiply the raw data by s_3^2 for regression analysis and check the fit after compensating this transformation. The desired effect of this transformation is a distortion of the statistical weights of the measured data points, yielding larger radii of convergence for the regression algorithm. On the other hand, this will cause a faint component of the system to become indeterminate due to the enlarged statistical noise in the outer part of the curve. As a compromise, a quadratic weighting function was applied so that the last data point was half the weight of the first.

The first step in data analysis was the verification that the density fluctuation background is not a signifi-

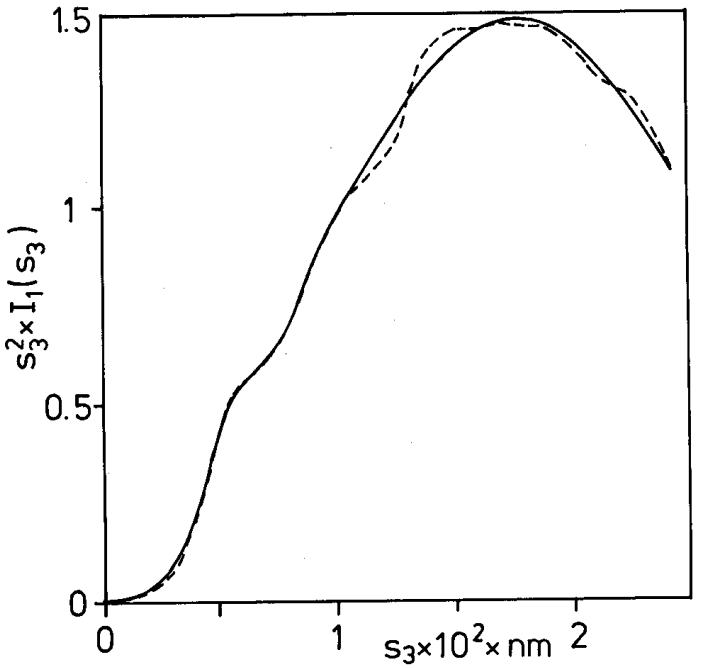

Fig. 6. Data (– – –) and fit (——) for double infinite stacking statistics on the interference function $s_3^2 \cdot I_1(s_3)$. The sample is a SBS block copolymer diluted with 50 wt % of paraffinic mineral oil at an elongation of $\lambda = 4$. Data were obtained from an axial section of the scattering pattern (see Fig. 1) close to the primary beam stop

Table 2. Fitted parameters for double fibrillar stacking statistics of an oil-diluted SBS copolymer (50 wt % of paraffinic oil) at an elongation of $\lambda = 4$

Parameter	value	interval of confidence
A_p, 1st stack	0.68	± 0.01
h_c [nm]	28	± 0
h_g [nm]	131	± 6
σ_1/h_c	0	
σ_2/h_g	0.39	± 0.03
A_p, 2nd stack	0.14	± 0.02
h_c [nm]	29	± 8
h_g [nm]	154	± 9
σ_1/h_c	1.6	± 0.5
σ_2/h_g	0.20	± 0.03

cant parameter. For this purpose the plain structural factor of a cylinder in axial direction was used as a model. This model is able to fit the coarse shape of the curve, neglecting the interparticular scattering. To this model a constant fluctuation parameter was added. It turned out that the latter parameter was iterated towards zero.

The next step was the use of Eq. (13) plus Eq. (14) ("two basic heights") with a series of 10 free varying σ_i parameters. The behavior of this series should help further model confinement. The result was the following series of σ_i/nm: (8, 59, 58, 55, 127, 108, 103, 63, 67, 61). Decreasing σ_i with increasing i show that there should be more than two basic heights in the sample. Unfortunately for this special set of data the quality of this statement is poor. But other curves (those without distinct layer lines) show the same behavior and good quality of the fit.

After that, the bimodal gap model (see Table 1) was tested. This model, as well, was not able to cure the lack of unreasonably decreasing σ_i (for the present curve, using the long index notation, e.g., $\sigma_{1213} = 150$ nm and $\sigma_{12131} = 100$ nm).

In the next step two parallel models were assumed. Because of the fact that the double model with freely varying σ_i shows strong correlations between parameters, the three basic models proposed (homogeneous L-distribution, paracristalline lattice, and stacking statistics) were instead tested in any combination. It turned out that the homogeneous L-distribution is not able to fit any of the curves, while it is difficult to distinguish between the two latter models. The model with double stacking statistics gave the best residual sum of squares, so it was used further on. All the data sets analyzed up to now can be excellently fitted with the double stacking model if the modulations due to possible layer lines are neglected.

Figure 6 shows the original data transformed to the interference function $s_3^2 \cdot I_1(s_3)$ and the best fitted curve for a double stacking statistics. The residual sum of squares for this fit is RSS = $4.6 \cdot 10^{-2}$ and the asymptotic correlation matrix shows one (reciprocal) correlation between the weights of the two components. The parameters of the fit are given in Table 2. Looking at the weights (i.e., A_p, Porod's asymptote) one can see that the main contribution to the scattering comes from the first stacking model. This model describes fibrils with excellently precise cylinder heights of 28 nm, so that the stacking statistic is solely caused by a 40 % variation of the gap heights. The second contribution to the scattering describes a stacking model with widely spread cylinder heights, but relatively well defined gaps (20 % variation).

Figure 7 shows the plot of the residual "interference function minus the fit" causing the layer lines. This residual cannot be fitted with any of the infinite models, but it strongly resembles of the scattering of a

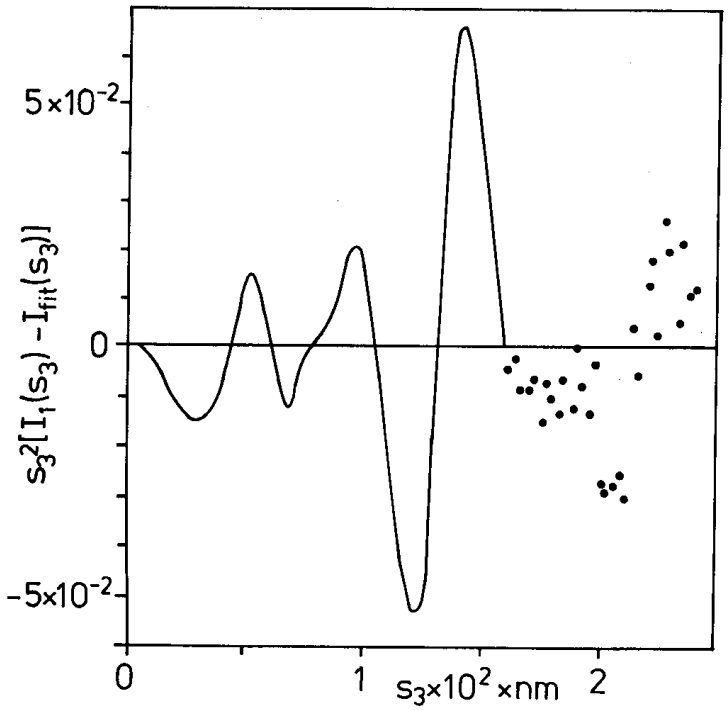

Fig. 7. Residual plot of a fit on the interference function $s_3^2 \cdot I_1(s_3)$, based on a double infinite stacking model (see Fig. 6)

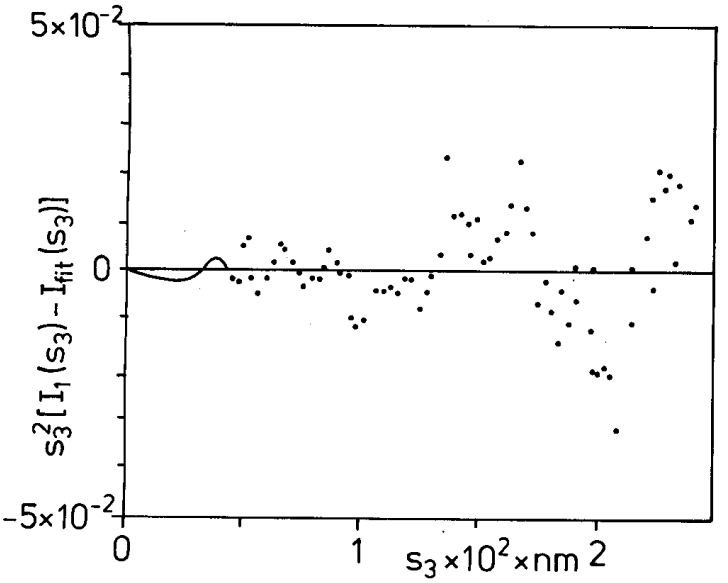

Fig. 8. Residual plot of a fit on the interference function $s_3 \cdot I_1(s_3)$, based on a four-fold model of two infinite, stacked fibrils and two string models

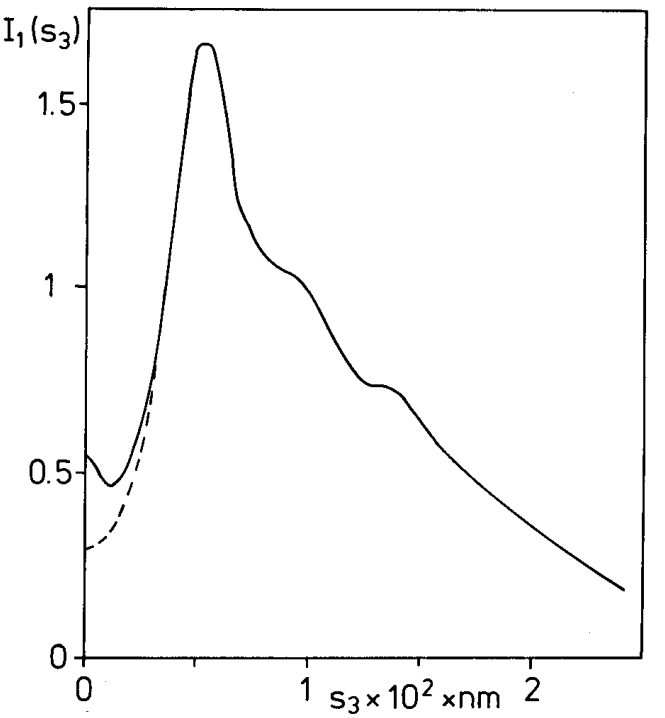

Fig. 9. Original scattering curve (- - -) and fitted function (——) based on a four-fold model of two infinite, stacked fibrils and two string models

string (see Fig. 4). Assuming one additional string model, RSS = $2.1 \cdot 10^{-2}$ is just halved with still a residual string model. Only after addition of a second string model (RSS = $5.6 \cdot 10^{-3}$) does the residual plot (Fig. 8) seem to closely represent the natural statistical noise of the experiment. Due to the transformation of the scattering curve this noise increases with s_3^2 in the residual plot.

A fitted and original scattering curve is plotted in Fig. 9, and Table 3 shows the final values of the regression parameters. The bad asymptotic intervals of confidence for the first string model are due to the correlated rest in the residual. This causes strong reciprocal correlations between A_p and h_c, as well as h_g and σ_1/h_c. Thus it was possible to get similar values of RSS for this component with smaller h_g but greater σ_1/h_c.

By adding a further model it was not possible to increase the quality of the fit for this curve. So the present parameter set seems to reflect the maximum of information to be obtained from data.

5. Interpretation

Against the background of the model developed in this paper the scattering pattern of the above thermoplastic rubber sample under elongation in progress can be described by two components of fibrils consisting of stacked cylinders with only short-range order. The main contribution to the pattern at $\lambda = 4$ is given by

Table 3. Fitted parameter for a four-fold model of two infinitely stacked and two finite stacked fibrillar components ("strings") of an oil-diluted SBS copolymer (50 wt% of paraffinic oil) at an elongation of $\lambda = 4$

Parameter	value	interval of confidence
A_p, 1st stack	0.66	± 0.08
h_c [nm]	28	± 0.7
h_g [nm]	141	± 1
σ_1/h_c	0	
σ_2/h_g	0.34	± 0.07
A_p, 2nd stack	0.11	± 0.01
h_c [nm]	27	± 3
h_g [nm]	169	± 1
σ_1/h_c	1.6	± 0.2
σ_2/h_g	0.10	± 0.05
A_p, 1st string	0.09	± 0.05
h_c [nm]	8	± 21
h_g [nm]	500	± 60
σ_1/h_c	0.27	± 1.4
σ_2/h_g	0.04	± 0.02
A_p, 2nd string	0.02	± 0.004
h_c [nm]	38	± 3
h_g [nm]	242	± 2
σ_1/h_c	0.37	± 0.11
σ_2/h_g	0	

cylinders with perfect heights of 28 nm and a shorter gap (140 nm). The second stacking model describes cylinders under destruction with a mean "height" of 27 nm and a wider gap (170 nm).

Anticipating the results of the whole series of curves with increasing elongation ratios, the first stacking model can be identified with cylinders standing upright in the direction of draw, while the other infinite stack contribution represents cylinders lying perpendicular to the drawing direction that are just breaking apart. Theoretical considerations concerning the latter component will be given in the following paper [12] on the whole sample series.

The two faint contributions to the pattern can be described by string models (just two PS-domains with a well-defined PB length in between). The component with the greater contribution describes PB chains that are stretched-out completely, while the other string with a gap of less than half the PB chain length can be explained by stretched-out chains penetrating the neighboring cylinder and then looping back to the starting cylinder. These two distances are well-defined due to the narrow molecular weight distribution of the PB-chain. So the perfect definition of a single distance that is not repeated causes many orders of layer lines to be observable.

The application of this method to an evidential subset of SBS block copolymers diluted with several kinds and amounts of mineral oil will be finished in the near future [12] and will give information on the variation of the superstructure as a function of draw ratio when drawing the thermoplastic rubber for the first time.

References

1. Polizzi S, Bösecke P, Stribeck N, Zachmann HG, Zietz R, Bordeianu R (1988) submitted to Polymer
2. Pakula T, Saijo K, Kawai H, Hashimoto T (1985) Macromolecules 18:1294–1302
3. Séguéla R, Prud'homme J (1988) Macromolecules 21:635–643
4. Ruland W (1977) Colloid Polym Sci 255:417–427
5. Stribeck N, Ruland W (1978) J Appl Cryst 11:535–539
6. Porod G (1951) Kolloid Z 124:103–114
7. Stribeck N, Ruland W (1982) poster presented on DPG spring conference, Regensburg
8. Porod G (1951) Kolloid Z 124:96–97
9. Caceci MS, Cacheris WP (1984) Byte 5:340–362
10. Draper NR, Smith H (1966) Applied Regression Analysis. John Wiley, New York, Chap 10, pp 263–306
11. Ceausescu E, Bordeianu R, Ghioca P, Buzdugan E, Stancu R, Cerchez I (1984) Pure & Appl Chem 56:319–328
12. Stribeck N, Bösecke P, Polizzi S, Zachmann HG, Ghioca P, Bordeianu R (1988) to be submitted to Colloid Polym Sci

Received July 4, 1988;
accepted October 25, 1988

Author's address:

Dr. N. Stribeck
Institut TMC
Bundesstr. 45
D-2000 Hamburg 13, F.R.G.